



ORIGINAL RESEARCH ARTICLE

Effect of Derivative Cutting of Flank-Faced Textured Ceramic Tools on Machined Surface

Jinxin Sun, Ran Duan, Quanjing Wang, Bing Qu, and Meng Wang

Submitted: 9 April 2024 / Revised: 28 May 2024 / Accepted: 17 June 2024

Surface microtexturing of the flank faces of tools is a promising way to improve the quality of machined workpiece surfaces. However, microtextures are often clogged in the process of machining because of the derivative cutting. The impact of derivative cutting on machined surface is frequently ignored. In this study, a microtexture was developed on the flank face of an Al_2O_3 ceramic tool, which paralleled to the cutting edge. The influence of derivative cutting on machined surfaces required to be systematically investigated according to surface roughness, surface topography, work hardening, and microstructural analysis. Results showed that derivative cutting occurred at cutting velocities ranging from 90 to 270 m/min, leading to an enhancement in the surface quality. Derivative cutting had an obvious impact on surface roughness, with the cutting velocity increased from 90 to 270 m/min. Furthermore, the bottom edge of the texture as a “cutting edge” can timely replace the main cutting edge of sudden failure, leading to the tool lives extension and surface quality improvement.

Keywords derivative cutting, machining, machined surface, metallography

1. Introduction

Over the past few years, the development of surface microtexturing on the flank face of tools has emerged as promising way to improve cutting performance and has received increasing attention (Ref 1-3). It can bring remarkable advantages, such as a decrease in the cutting force (Ref 4-6), enlargement of the heat transfer area (Ref 7, 8), improvement of anti-wearability (Ref 9, 10), as well as enhancement quality of machined surface (Ref 11). Ze et al. (Ref 12) created a flank-faced textured tool for machining Ti-6Al-4V, and their results showed that the fabricated tool had small cutting forces during the machining process, compared to the conventional cutting tool. Fatima et al. (Ref 10) machined AISI/ASE using flank-faced textured tools. They indicated that the flank-faced textured tools had a significant effect on reducing the cutting force. Sanjib et al. (Ref 13) conducted a study on the cutting performance of tools with texture flank face. Their research revealed that the depth of the white layer on the workpieces machined using these textured tools was considerably reduced. Meanwhile, compare with conventional tools, the flank-faced textured tools had a decrease cutting force. According to Muhammed et al. (Ref 14), workpieces machined

with tools featuring flank face microtexturing exhibited lower surface roughness compared to those machined with conventional tools. Tatsuya et al. (Ref 15) created flank-faced textured tools to suppress the failure of the main cutting edge. Ranjan and Hiremath (Ref 16) studied the influence of flank-faced textured on the cutting performance of tools. They reported that the flank-faced textured tools exhibited a reduction in the feed and tangential forces. Research has demonstrated that the microtexture applied to the flank face of tools can significantly improve their cutting performance.

Although several benefits of flank-faced textured tools have been clarified, microtextures are always clogged in the process of machining owing to derivative cutting. Derivative cutting means the additional cutting of chips by the edge of microtexture (Ref 16). Derivative cutting at the rack face enhances the plowing action at the chip. This action diminished the wear resistance of the tool surface (Ref 17). This leads to a poorly machined surface. However, Liu et al. (Ref 18) created a flank-faced textured cemented carbides tool. They found that the uneven defects on the machined surface could be removed by derivative cutting, leading to an improvement in the quality of machined surface. Moreover, derivative cutting efficiently alleviated tool wear. Xu et al. (Ref 19) reported that flank face microtexturing tools could remove protuberances on the machined surface, which resulting in a decrease in surface roughness of workpieces.

According to the literature, the derivative cutting of microtextured tools on the flank face can have an impact on the machined surface. Researchers mostly attribute the improvement in the quality of the machined surface by microtextured tools to their friction-reducing and lubricating effects, and derivative cutting is often overlooked. Therefore, derivative cutting on a flank face requires systematic research. In this study, an Al_2O_3 ceramic tool with a microgroove on the flank face was created. Since multiple microtextures can have a significant impact on cutting temperature, stress distribution, and cutting force, which in turn affects the occurrence of

Jinxin Sun, Ran Duan, and Quanjing Wang, School of Mechanical and Electronic Engineering, Shandong Jianzhu University, No. 1000 Fengming Road, Jinan 250101 Shandong, People's Republic of China; Bing Qu and Meng Wang, Shandong Xinchuan Mine Mechanical and Electrical Equipment Co., Ltd, Jining 272000 Shandong, People's Republic of China. Contact e-mail: duanran20@sdjzu.edu.cn.

derivative cutting. A linear microgroove can exclude the influence of those factors on the derivative cutting. The microgroove was paralleled to the main cutting edge. Conventional and newly fabricated tools were selected to machined AISI 1045. The effect of derivative cutting on machined surface was explored.

2. Experimental Procedures

2.1 Fabrication of Microtextured Tools

The $\text{Al}_2\text{O}_3/\text{TiC}$ ceramic tool SNGN 120408 (Zibo Dongtai Co. Ltd., China) with a 0.8 mm tool tip radius was selected for

surface microtexturing in this experiment. Table 1 shows the physical properties and element composition of the tools. A fiber laser (Coherent Inc.) with a wavelength of 800 nm, repetition rate of 1000 Hz, and pulse width of 120 fs was selected to fabricate a flank-faced microtextured tool. The microtexture was prepared by scanning speed of $300 \mu\text{m/s}$ and a frequency of 1000 Hz of the processing parameters of laser. According to previous studies (Ref 19-22), the size parameters of microtexture were designed. Results showed that incorporating microtexturing on the flank face of tools could enhance cutting performance, but showed a phenomenon of derivative cutting under those parameters. For this reason, the length of the microtexture was selected approximately $300 \mu\text{m}$, the depth of the microtexture was approximately $38 \mu\text{m}$. The distance

Table 1 Properties of SNGN 120408 (Ref 23)

Composition, wt.%	Hardness, HV	Density, g cm^{-3}	Fracture toughness, $\text{MPa m}^{1/2}$	Flexural strength, MPa
$\text{Al}_2\text{O}_3/55\text{TiC}$	2400	4.76	5.04	900

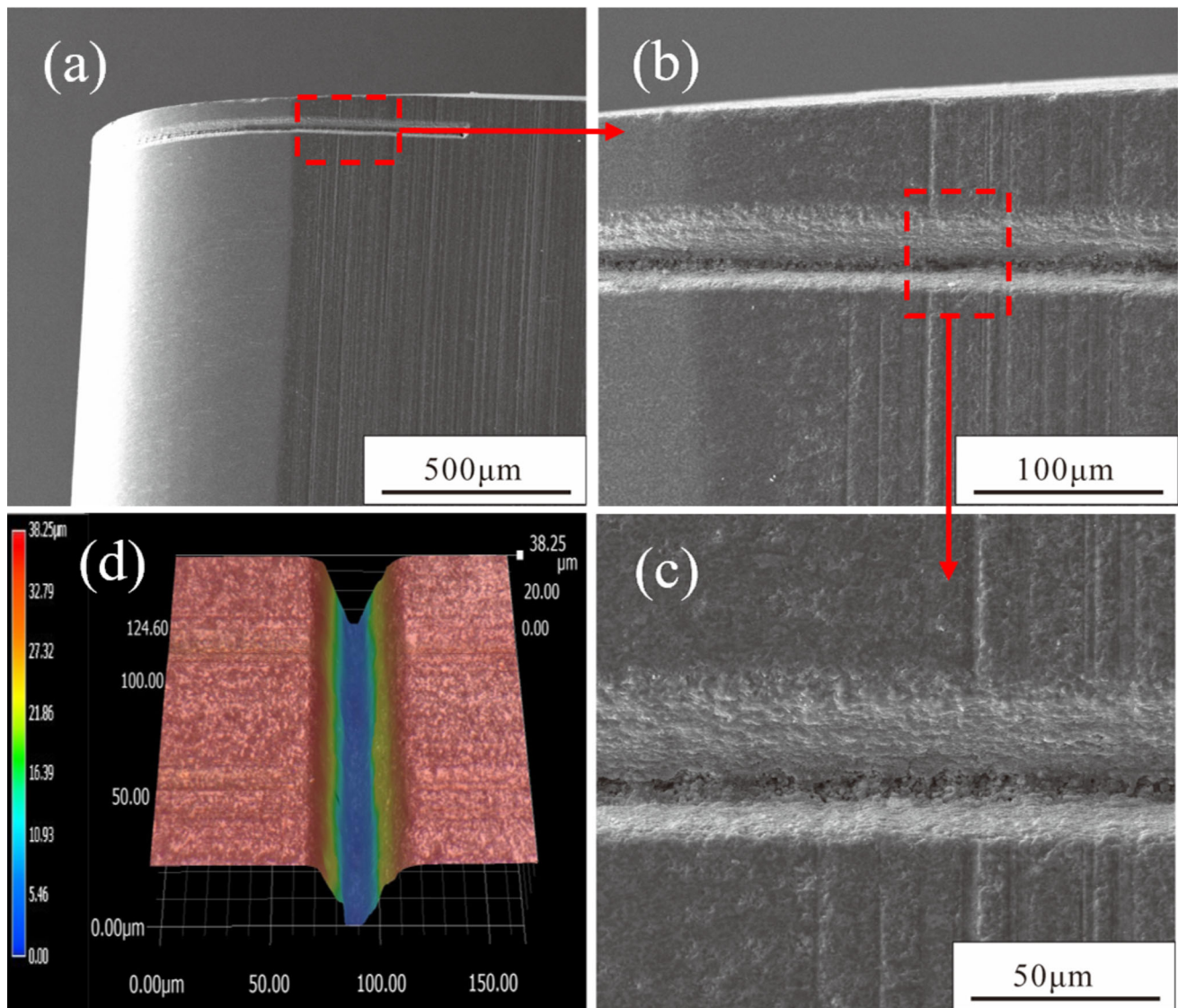


Fig. 1 Micrographs and 3D profile of the microgroove

from the microtexture to the main cutting edge measured 50 μm . The angles of the bottom edge of texture are consistent. Figure 1 illustrates the topographies of the newly fabricated tool. As depicted in Fig. 1(c), the surface of microtexture groove is smooth, and there is no residual material produced by laser machining in it. Thus, the influence of other factors on derivative cutting is eliminated. The 3D profile of the microgroove is shown in Fig. 1(d). A flank-faced textured tool named TT and a commercial SNGN 120408 named CT were used for the dry cutting experiment.

2.2 Cutting Experiments

A CA 6140 lathe (Jinan First Machine Tool Co. Ltd., China) was selected to the turning experiment of AISI 1045. The CA 6140 was furnished with a normal tool holder, in which the cutting edge, the flank angle and the inclination angle are 45, 8, 0° respectively. The cutting workpiece was a cylindrical bar of AISI 1045 with a diameter of 100 mm, and the cylindrical bar was with a hardness of HV 300. The tensile strength is between 115 and 234 MPa, the yield strength is 23 MPa, and the elongation rate is greater than 65%. Table 2 shows the chemical composition of the AISI 1045 steel. Figure 2 shows the microstructure of the workpiece. The selection of cutting parameters was based on the previous studies (Ref 24), and the results indicated that the fabricated tools showed a stable phenomenon of derivative cutting under those parameters. Therefore, the cutting velocity ranged from 90 to 270 m/min. A cutting depth of 0.5 mm was chosen, and a feed rate set at 0.36 mm/rev. The cutting distance was 100 mm. A scanning electron microscopy (SEM, QUANTA FEG 250, FEI Inc.,

Table 2 Chemical constituents of AISI 1045 steel, wt.%

Si	Cr	Mn	C	Fe
1.28	0.5	1.71	0.4	Bal.

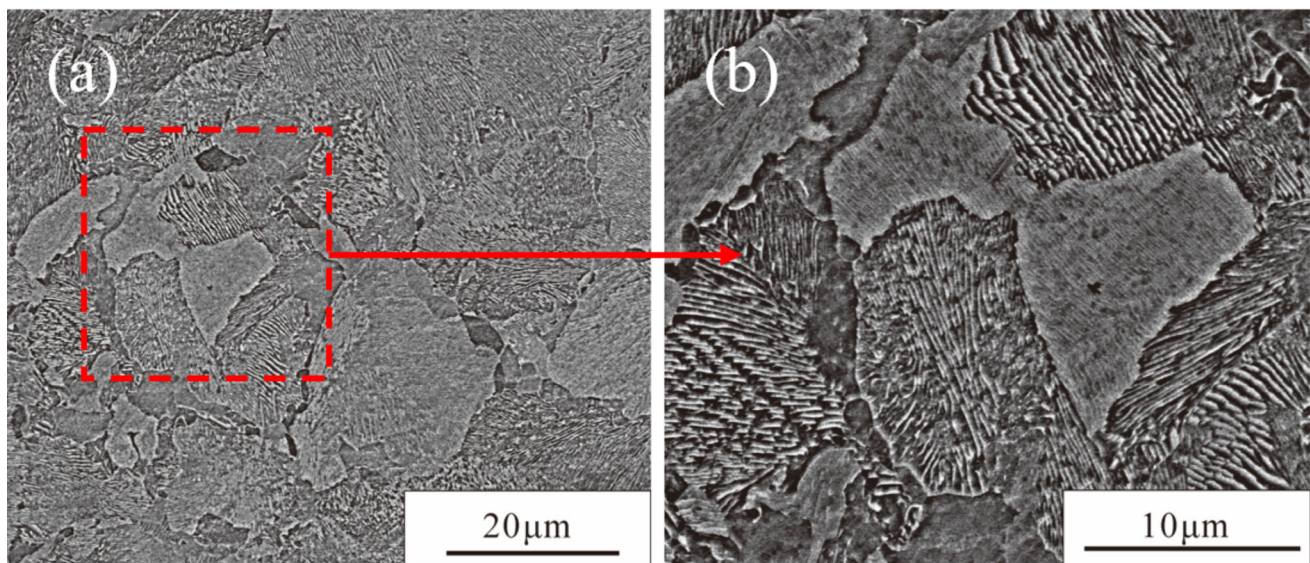


Fig. 2 Microstructure of AISI 1045

USA) was selected to examine morphologies of the worn regions of the cutting tools and microstructure of the workpiece. X-ray spectrometry was selected to analyze the chemical composition contained in the derivative chips. The 3D morphologies of the surface of tools and surface morphologies of AISI 1045 were examined using a super depth-of-field microscope (VHX-5000, Keyence Co., Ltd.). A Vickers microhardness tester (HV-1000STA, Laizhou Weiyi Experimental Machine Manufacturing Co. Ltd., China) was used to examine the hardness of the surface of workpiece after processing. To minimize experimental variability, each experiment was conducted five times, with the average values being given.

3. Results and Discussion

3.1 Topography of the Flank Face of CTs and TTs

Figures 3, 4, 5, 6 show the morphologies and chemical compositions (point 1) of the CTs at 100 mm after cutting at velocities changing from 90 to 270 m/min, respectively. At a cutting velocity of 90 m/min, intensive chipping occurred in the flank face of CT. As depicted in Fig. 3(b), an extensive adhesion layer was prominently visible within the wear area. The adhesion layer contained several Fe elements, as depicted in Fig. 3(c) and (d). A minor degree of adhesion was noted on the flank face, as evidenced by Fig. 4. In Fig. 5, it was evident that an increase in cutting velocity to 211 m/min led to a heightened level of adhesion on the flank face. The presence of adhesive material was distinctly visible on the flank face, which we could observe in Fig. 6(b). Additionally, Fig. 6(c) indicates that the flank face had a large amount of Fe.

Figures 7, 8, 9, 10 show the morphologies and chemical compositions (point 1) of the TTs at 100 mm after cutting at velocities changing from 90 to 270 m/min, respectively. Figure 7(b) reveals the presence of significant chipping within the cutting zone. The bottom edge of the texture was adhered by derivative chips. Figure 7(c) shows that Fe was distributed

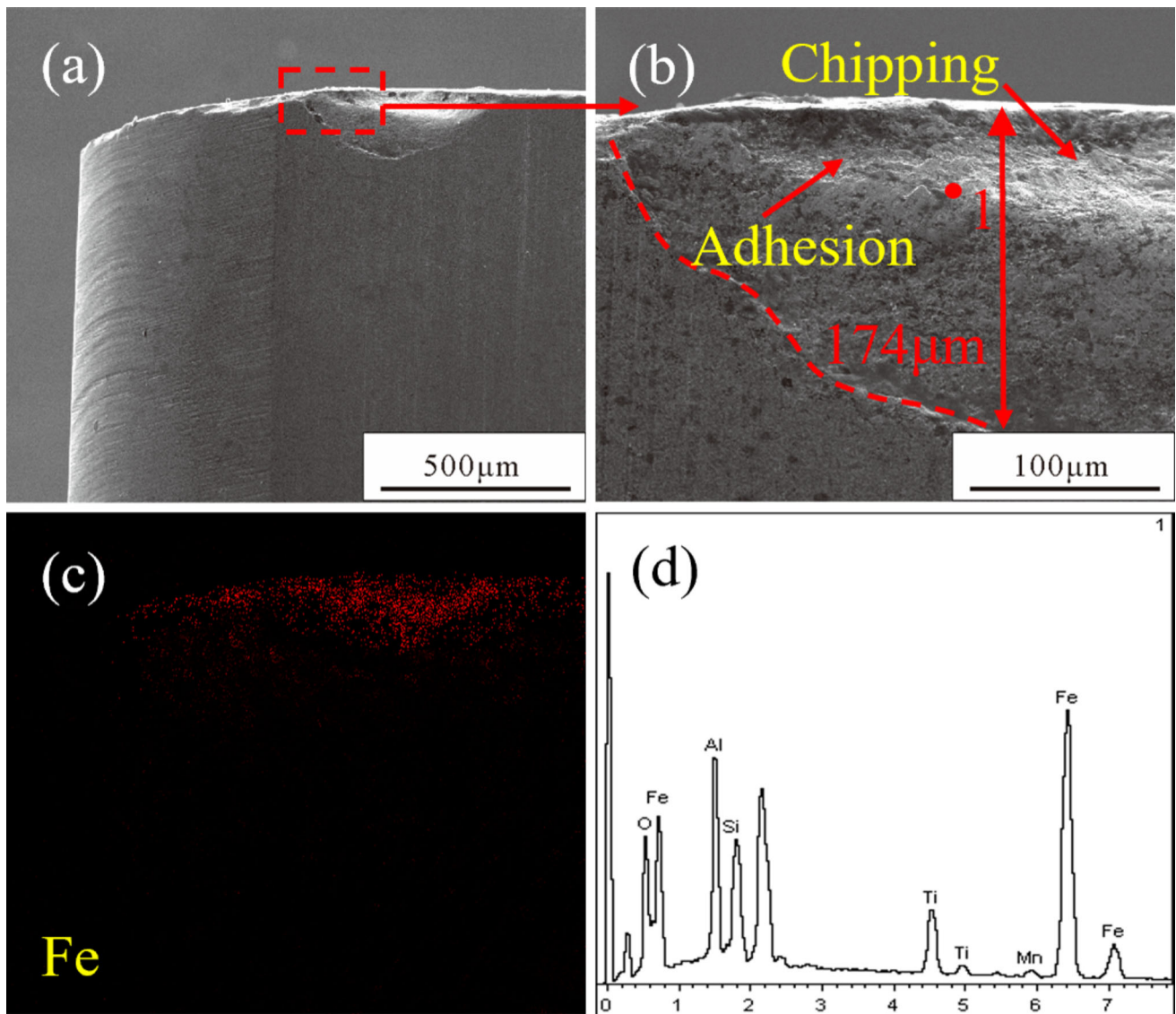


Fig. 3 After machining topography and elemental analysis of the CT at 90 m/min. (a) SEM micrographs, (b) magnified view of (a), (c) Fe distribution in (a), and (d) point 1 elemental analysis

near the microtexture. Moreover, the EDX analysis at point 1 revealed a substantial concentration of Fe in the derivative chips, as displayed in Fig. 7(d). Based on the chemical composition examination and the EDX mapping of Fe on the microtextured are shown in Fig. 8 and 9, there was a small

amount of Fe in the microtexture. Figure 10 shows that chipping and cracking occurred in the cutting zone. This could be due to the short distance between microtexture and main cutting edge, which affected the robustness of the cutting zone of the TT. The microtexture was plugged by derivative chips, as

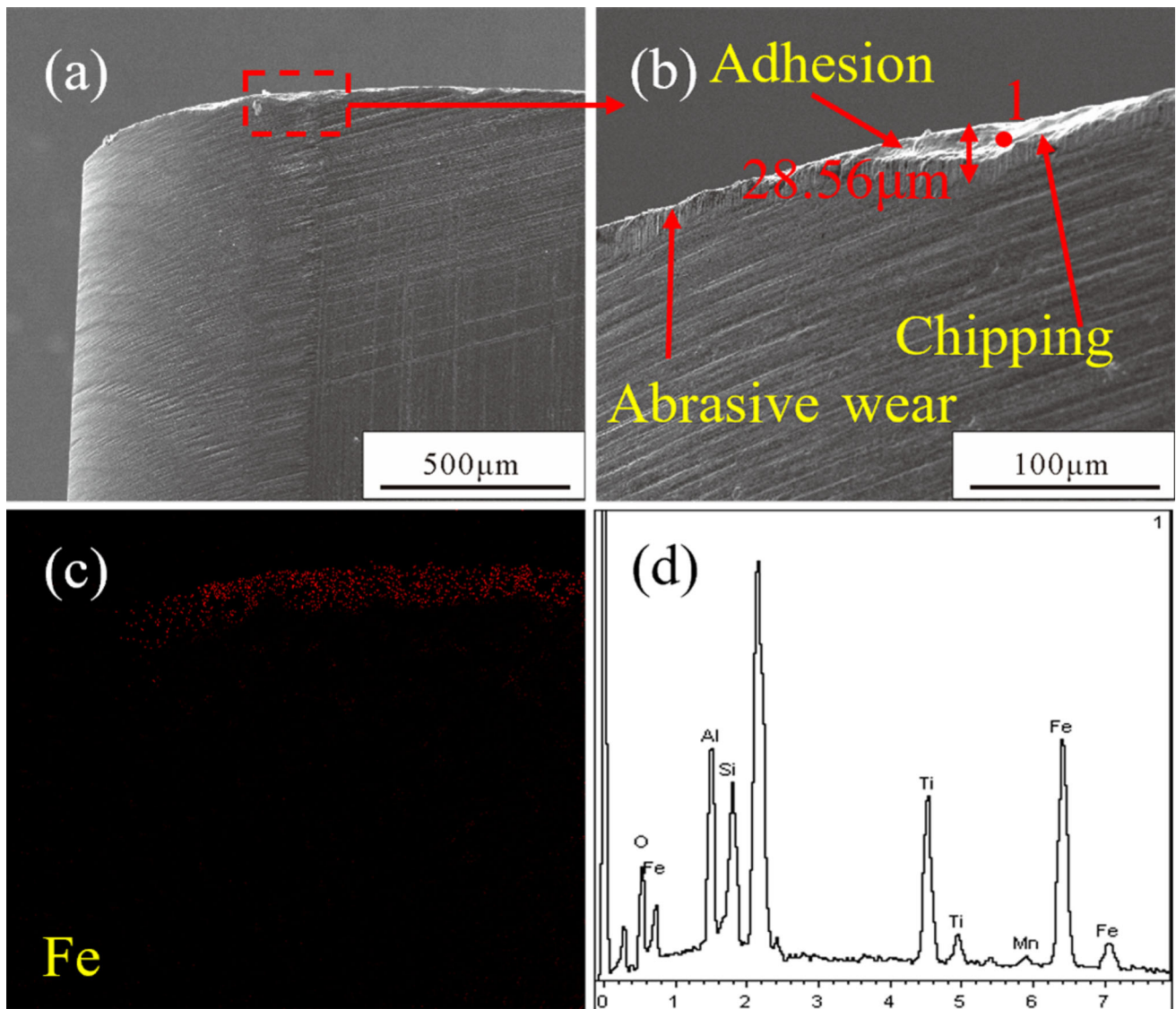


Fig. 4 After machining topography and elemental analysis of the CT at 133 m/min. (a) SEM micrographs, (b) magnified view of (a), (c) Fe distribution in (a), and (d) point 1 elemental analysis

shown in Fig. 10(b). Numerous plowing grooves were discernible in proximity to the microtexture region, a result of derivative cutting, which elevated the interface temperature between the tool and the workpiece. The temperature rise

induced a decrease in the wear resistance of the textured area (Ref 25). In addition, there were large amounts of Fe in the derivative chips, as shown in Fig. 10(c) and (d). The occurrence and distribution of adhesion on the cutting tool face has been

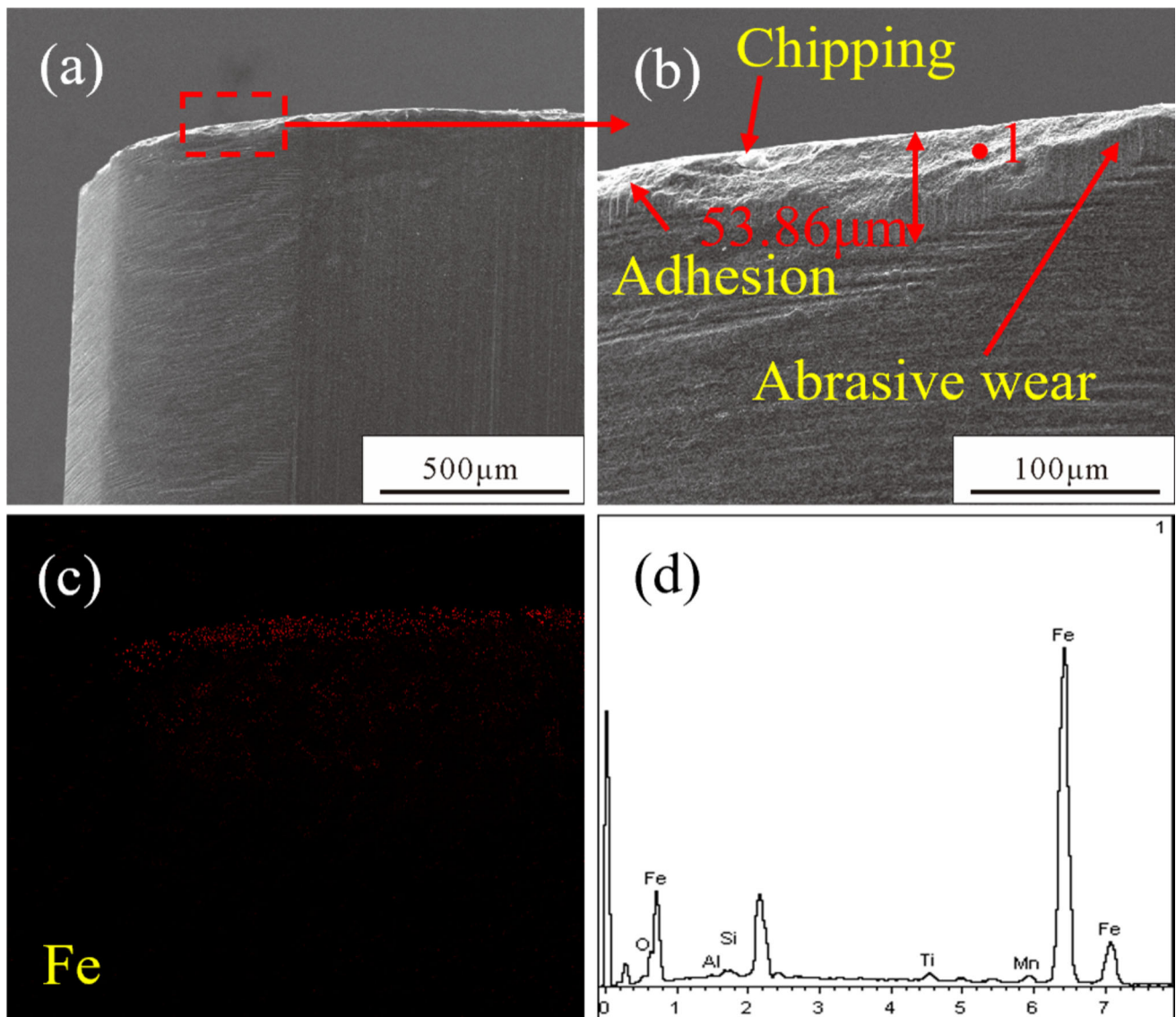


Fig. 5 After machining topography and elemental analysis of the CT at 211 m/min. (a) SEM micrographs, (b) magnified view of (a), (c) Fe distribution in (a), and (d) point 1 elemental analysis

qualitatively identified by EDX in previous studies (Ref 26, 27). The Fe distributions shown in Figs. 3(c), 4(c), 5(c) and 6(c) indicated that the adhesion on the surface of tools increased as the cutting velocity was elevated within a range of 90 to 270 m/min. The adhesions on the flank face of the TTs were greater than those on the flank faces of the CTs.

3.2 Flank Wear of the Tool

The variations in flank face wear with cutting velocity obtained using the CTs and TTs as shown in Fig. 11. As depicted in the figure, there was a notable reduction in flank wear for both the CTs and TTs when the cutting velocity was maintained between 90 and 133 m/min. Subsequently, as the

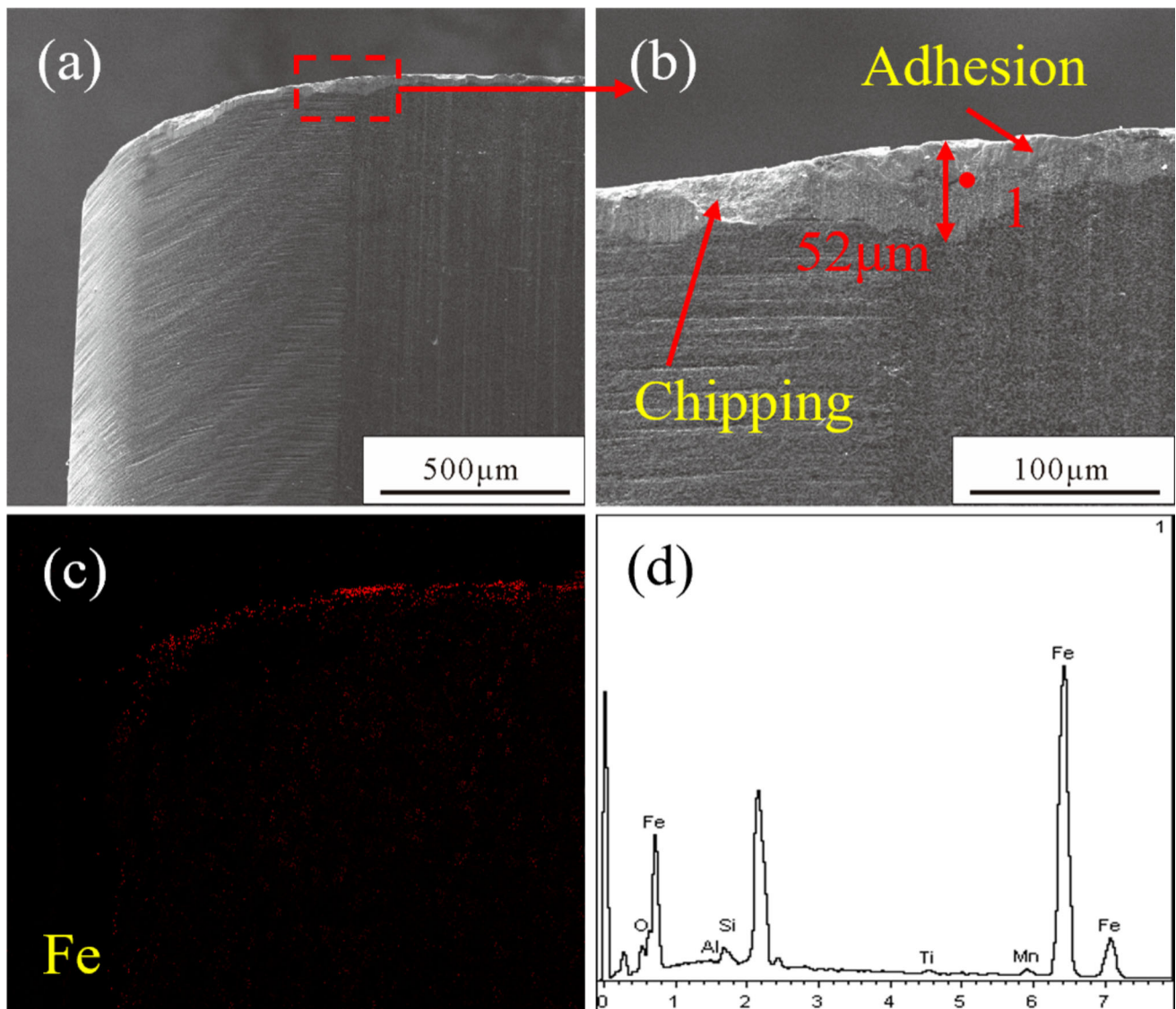


Fig. 6 After machining topography and elemental analysis of the CT at 270 m/min. (a) SEM micrographs, (b) magnified view of (a), (c) Fe distribution in (a), and (d) point 1 elemental analysis

cutting velocities increased from 133 to 270 m/min, there was a notable upward trend in the flank face wear for both the CTs and TTs. The TTs showed higher flank wear resistance than the CTs when the velocity was less than 211 m/min. However, the flank face wear of the CT was lower than that of the TT at 270 m/min because of intensive derivative cutting.

3.3 Surface Roughness and Surface Topography

Figures 12, 13, 14, 15 show the surface topography with CTs of 100 mm after machining at cutting velocities that vary between 90 and 270 m/min, respectively. Figure 12 illustrates that the predominant defect type on the machined surface were

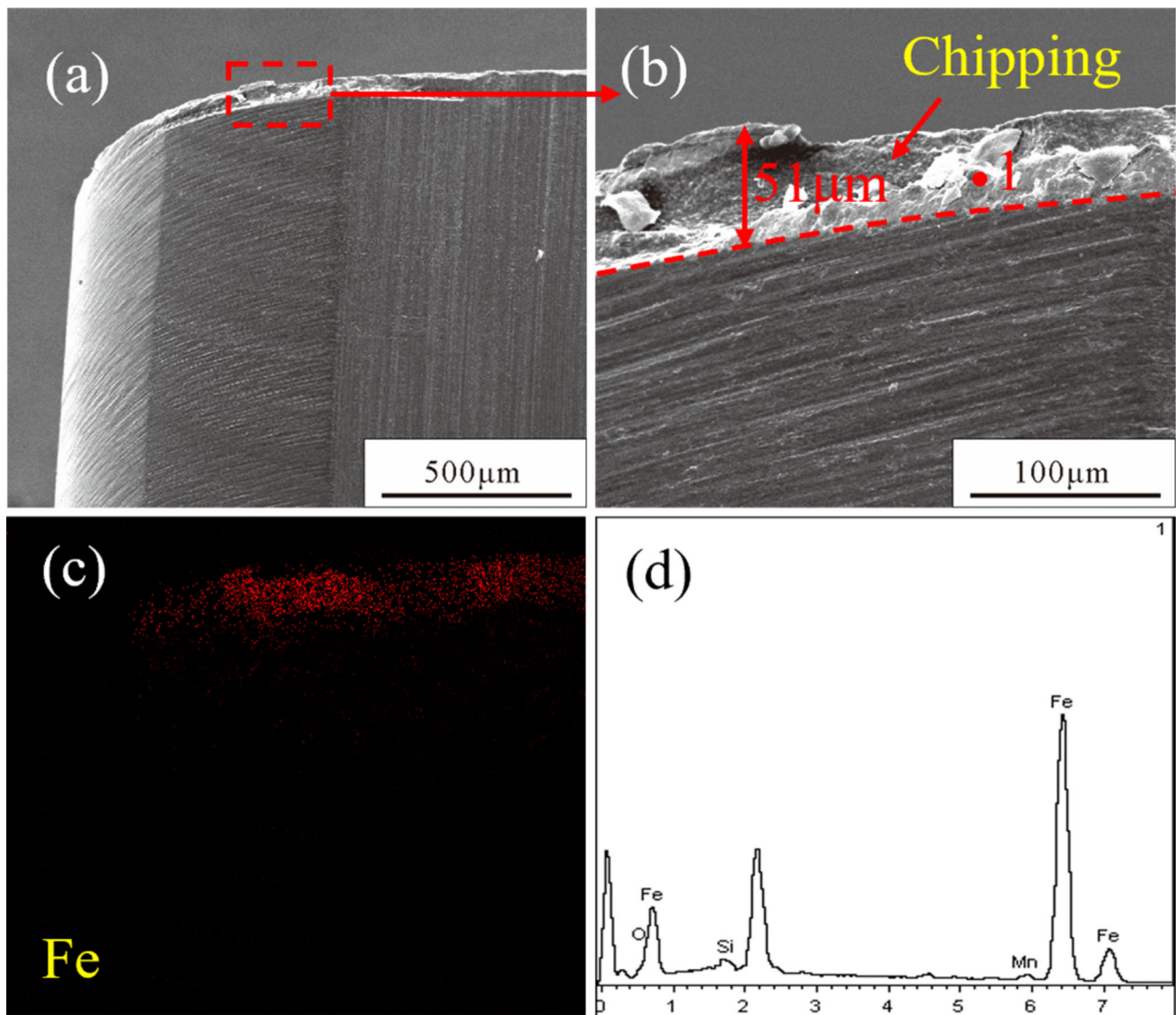


Fig. 7 After machining topography and elemental analysis of the TT at 90 m/min. (a) SEM micrographs, (b) magnified view of (a), (c) Fe distribution in (a), and (d) point 1 elemental analysis

plowing grooves when the cutting velocity was 90 m/min. Figures 13, 14, 15 illustrate that the defects on the machined surface were mainly protuberances. As the cutting velocity rose, there was a corresponding increase in the quantity of bonding materials observed on the machined surface increased.

Figures 16, 17, 18, 19 show the surface topography with TTs of 100 mm after cutting at velocities ranging from 90 to 270 m/min, respectively. The workpiece surfaces machined with the TTs were smooth, and there were no significant machining defects, as shown in Figs. 16, 17, 18, 19. Feed marks were only

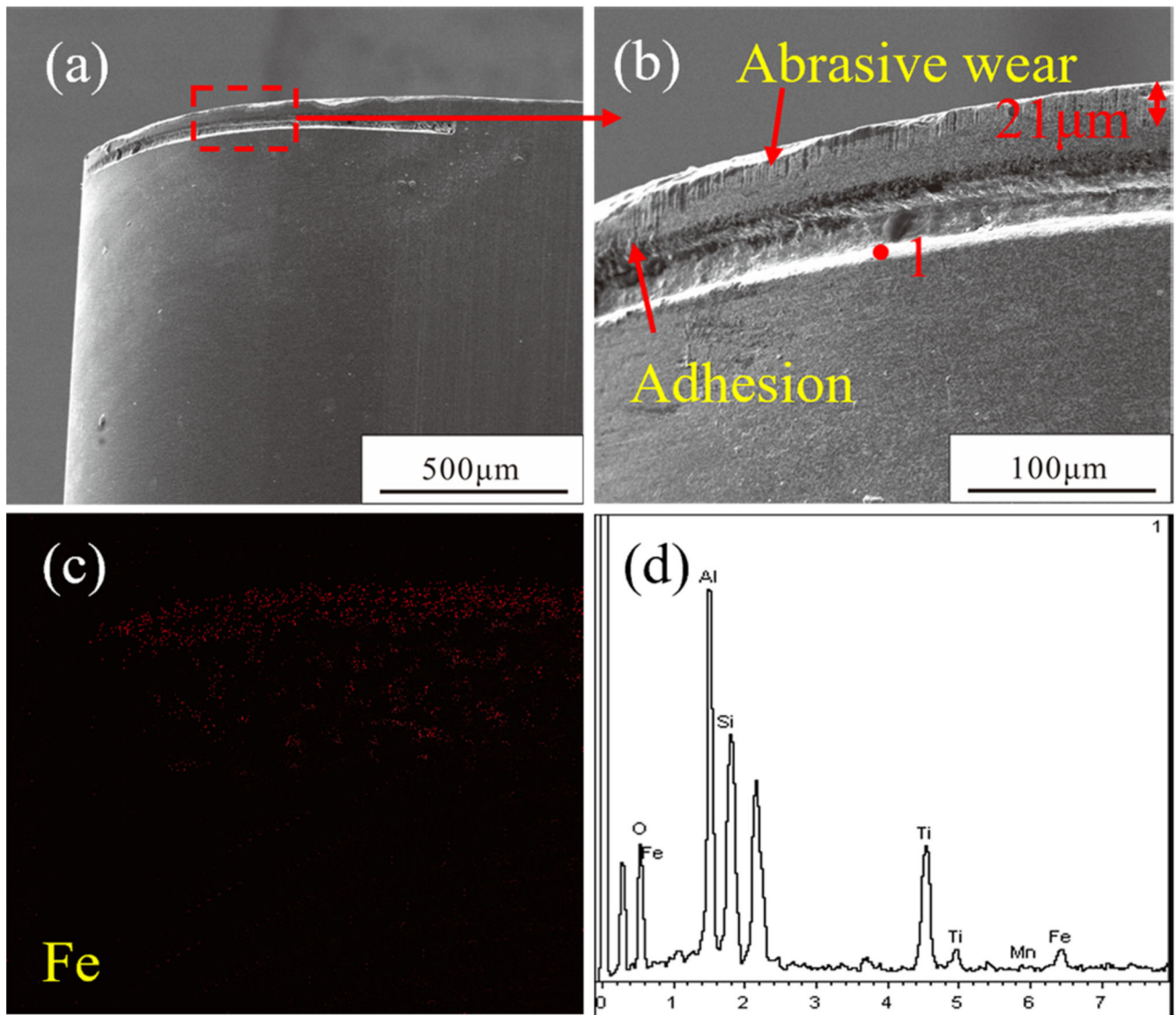


Fig. 8 After machining topography and elemental analysis of the TT at 133 m/min. (a) SEM micrographs, (b) magnified view of (a), (c) Fe distribution in (a), and (d) point 1 elemental analysis

present on the surface. These are common phenomenon that occur surfaces. The feed marks became insignificant with the rise in cutting velocity from 90 to 270 m/min.

Figure 20 shows the variations in surface roughness with the cutting velocity obtained using the CTs and TTs. From this figure, we could see that the surface machined by CTs exhibited

higher surface roughness than the surface machined by TTs. The difference in the surface roughness between the surfaces machined using the TTs and CTs widened as the cutting velocity incremented. At cutting velocities from low to high, the surface roughness of the workpieces worked with the TTs decreased by approximately 22, 77, 325 and 645%, respec-

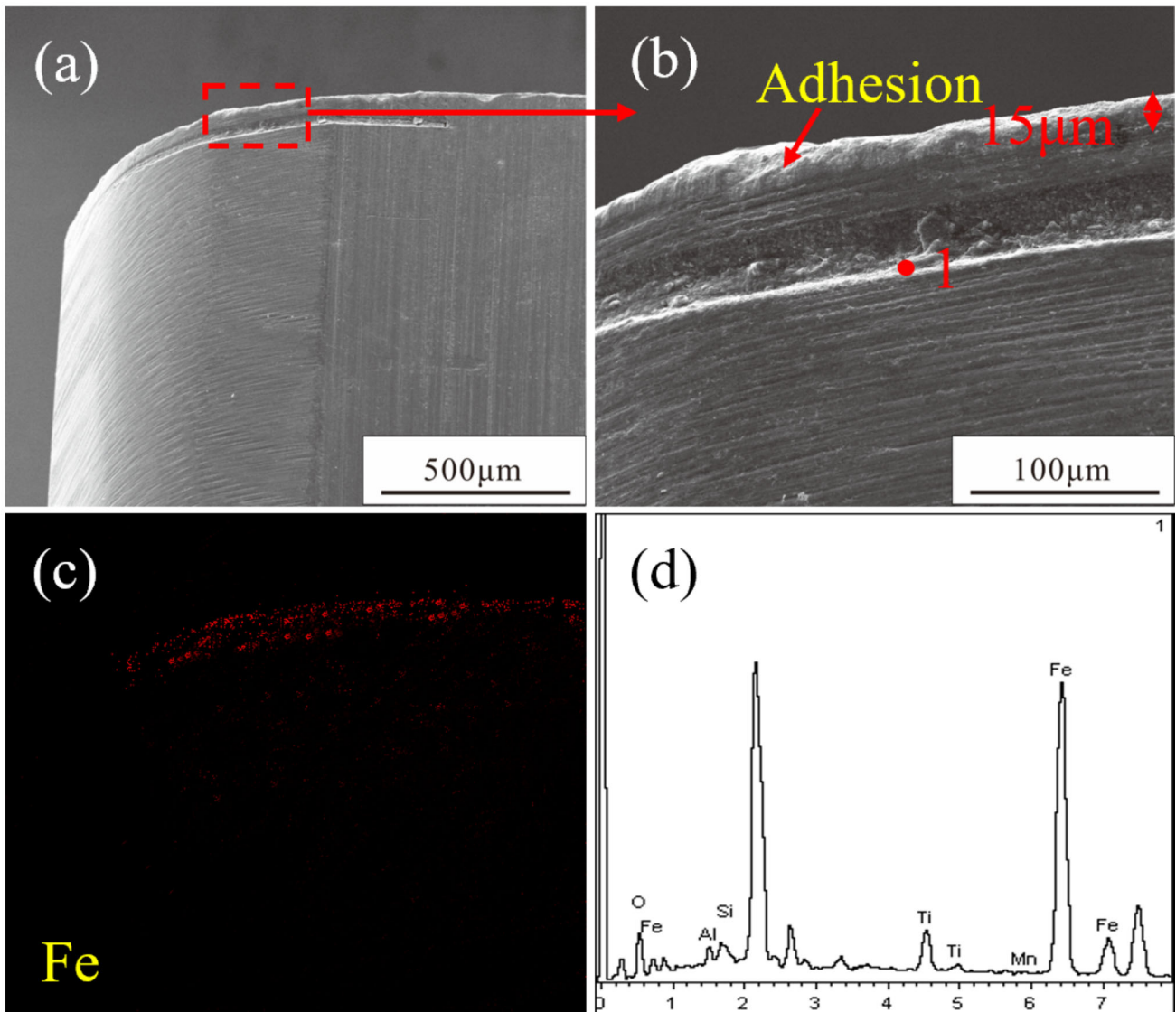


Fig. 9 After machining topography and elemental analysis of the TT at 211 m/min. (a) SEM micrographs, (b) magnified view of (a), (c) Fe distribution in (a), and (d) point 1 elemental analysis

tively, compared with that of the workpiece machined by the CTs. In addition, for the surface machined by the TTs, the surface roughness exhibited a decreasing trend across the cutting velocity spectrum of 90 to 270 m/min.

3.4 Microstructure of the Workpiece Material

Figure 21 shows micrographs of the subsurface microstructure with CTs at different velocities. As for the workpiece machined by the CTs, when the velocity was 133 m/min, the

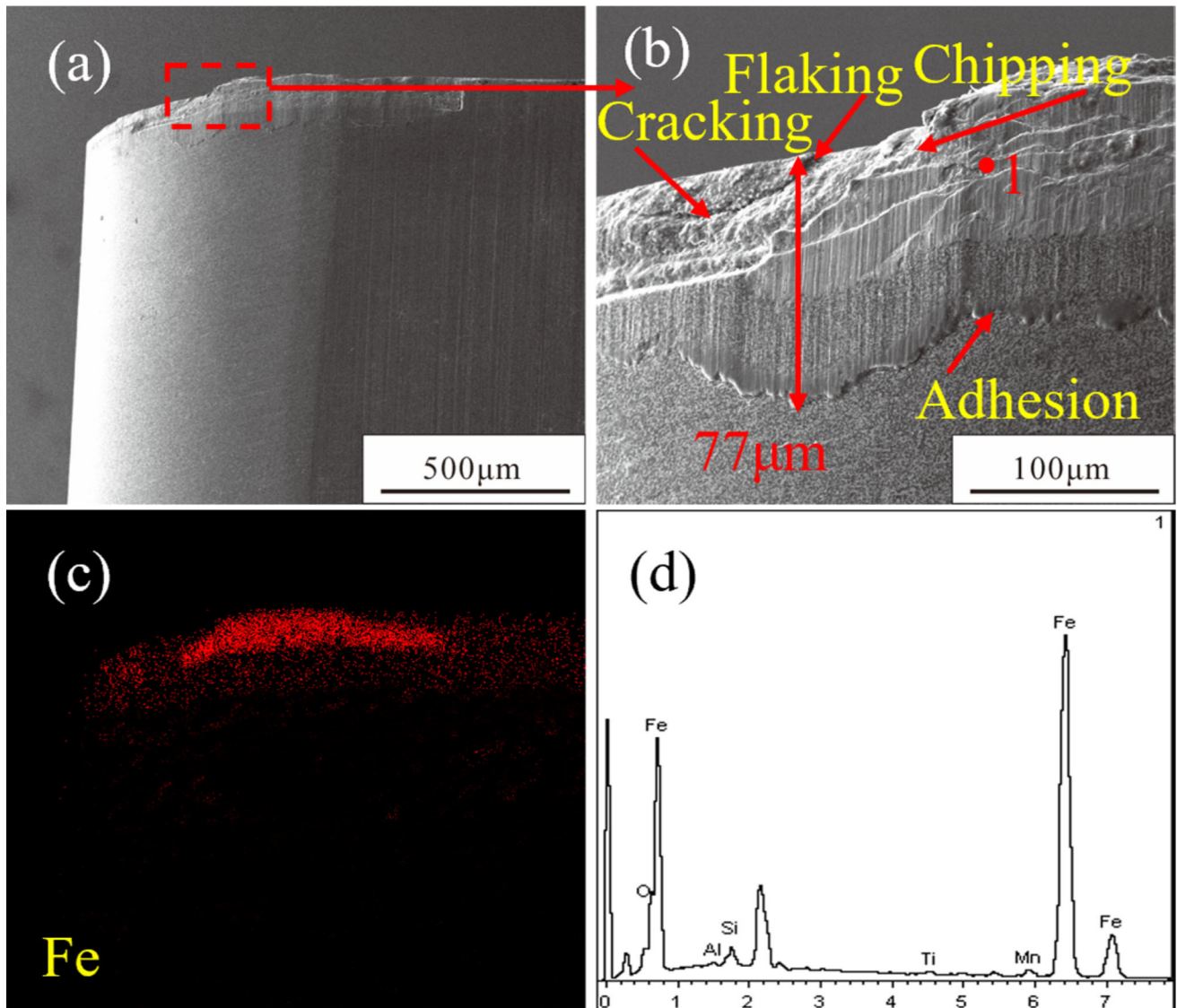


Fig. 10 After machining topography and elemental analysis of the TT at 270 m/min. (a) SEM micrographs, (b) magnified view of (a), (c) Fe distribution in (a), and (d) point 1 elemental analysis

maximum depth of fine grain zone was $3.84 \mu\text{m}$. The minimal depth of fine grain zone was $1.8 \mu\text{m}$ at 211 m/min. The asymptote lines delineated the plastic deformation in relation to

the direction of the cutting velocity (v). The orientation of plastic deformation aligns with the trajectory of the cutting velocity.

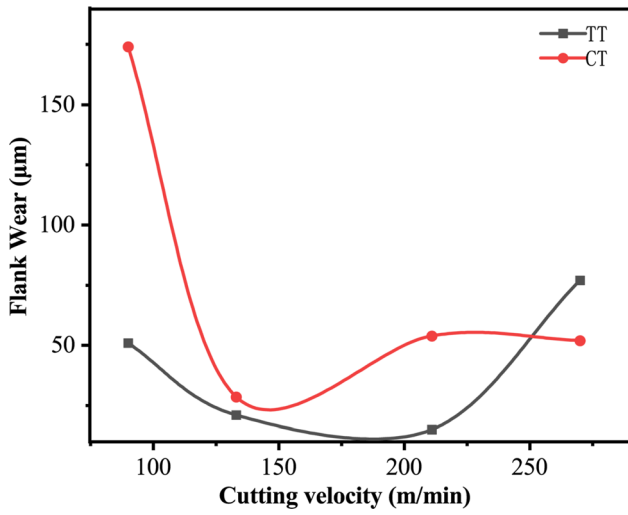


Fig. 11 Flank face wear of the TTs and CTs in dry cutting of AISI 1045

Figure 22 shows micrographs of the subsurface microstructure with TTs at different velocities (v). As for the workpiece machined by the TTs, when the velocity was 90 m/min, the maximum depth of fine grain zone was $3.8 \mu\text{m}$. The minimal depth of fine grain zone was $0.93 \mu\text{m}$ when the velocity was 133 m/min. The depth of the fine grain zone showed an increasing trend as the cutting velocities increased within the range of 133 to 270 m/min. Compare Fig. 21 with Fig. 22, we can see that the thickness of the fine grain zone of the surface machined by the TTs is smaller than that of the surface machined by the CTs at velocities ranging from 133 to 270 m/min.

3.5 Hardness

The hardnesses of the workpieces obtained using the CTs and TTs were measured. The test parameters were a 100 gf load and 12 s holding time. Hardness was measured in five repeated experiments to gain average values. The hardness of the workpiece increased with cutting velocities ranging from 90 to

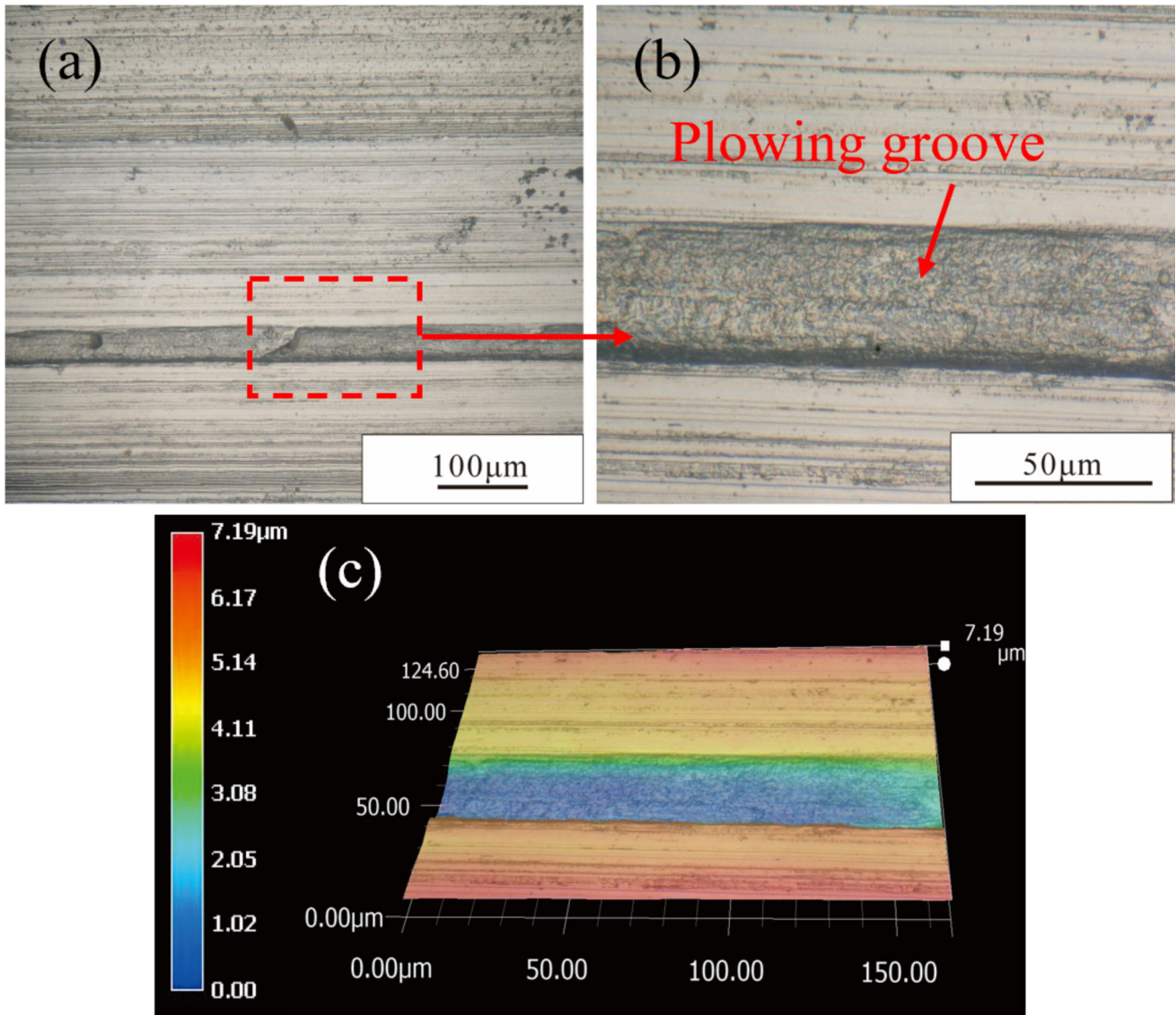


Fig. 12 Surface topography with CT at 90 m/min. (a) Surface topography, (b) magnified view of (a), and (c) 3D profile of (b)

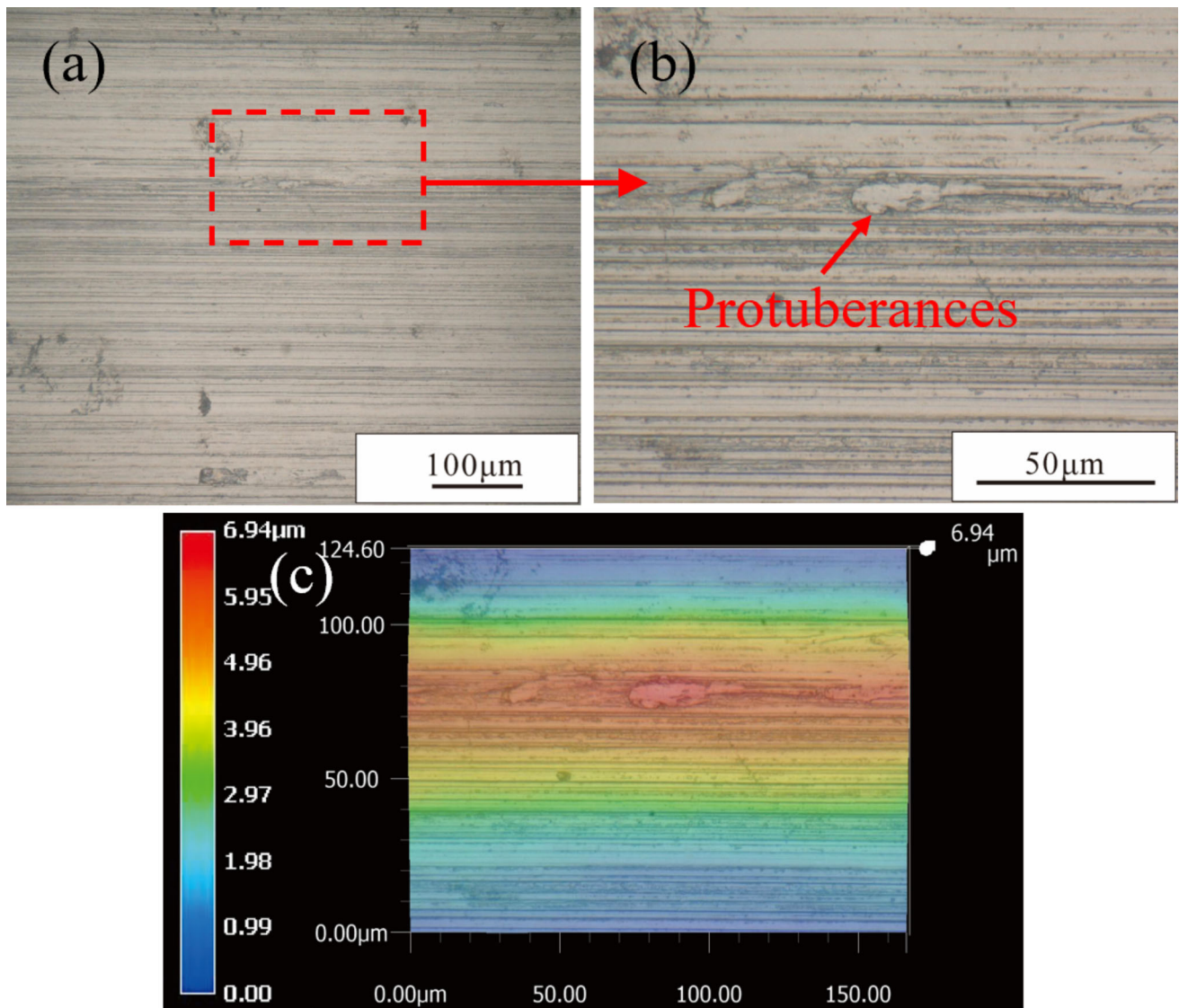


Fig. 13 Surface topography with CT at 133 m/min. (a) Surface topography, (b) magnified view of (a), and (c) 3D profile of (b)

270 m/min. Figure 23 shows the hardness of the workpieces machined using the CTs and TTs at various cutting velocities. It was observable that the hardness of the workpiece machined by the CT were higher than that of the workpiece machined by the

TT at 90 m/min. In addition, the hardness of the workpiece machined using the TTs was lower than that of the workpiece machined using the CTs within the cutting velocity interval of 133-270 m/min. From low to high cutting velocities, the

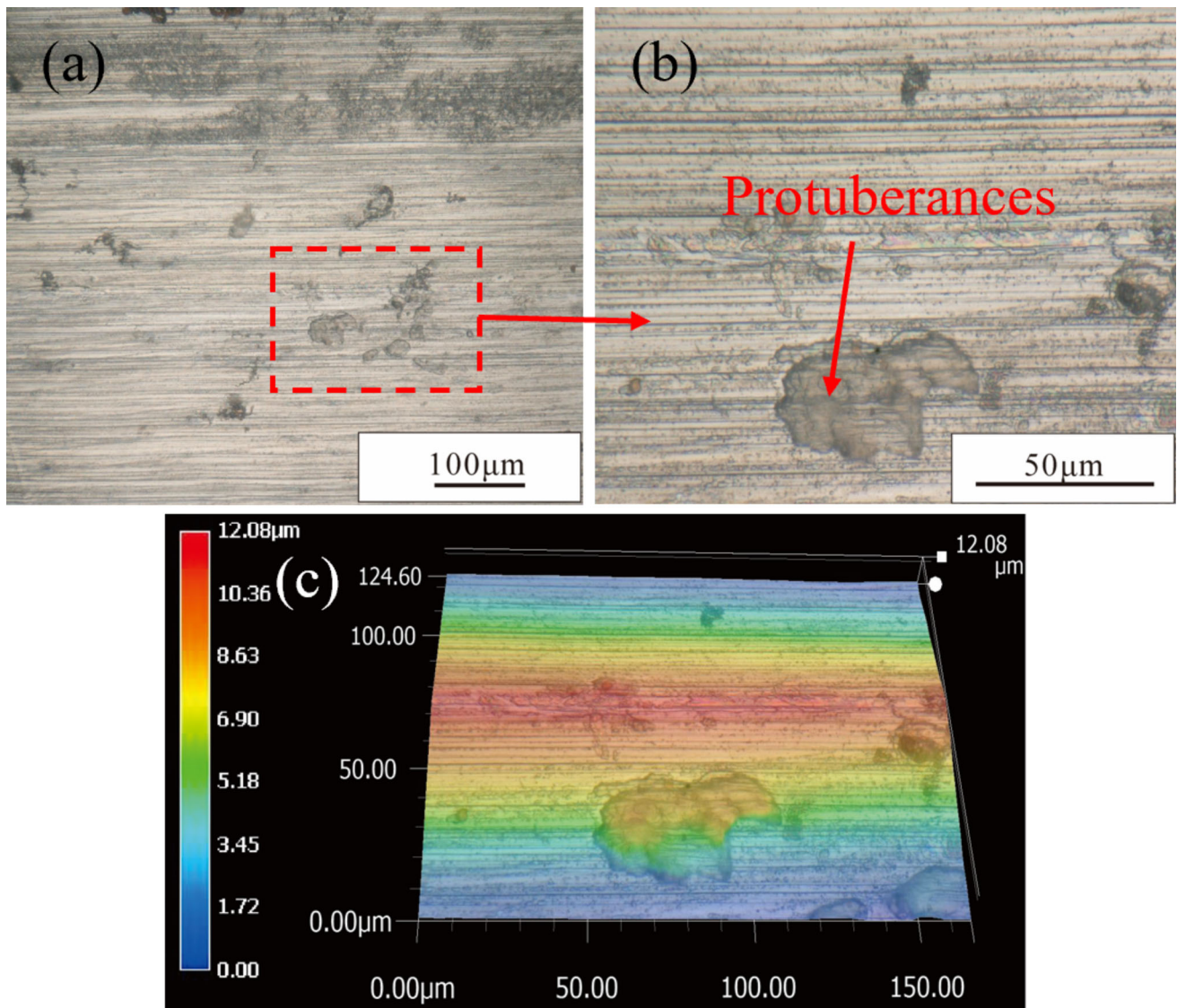


Fig. 14 Surface topography with CT at 211 m/min. (a) Surface topography, (b) magnified view of (a), and (c) 3D profile of (b)

difference in the hardness of the surfaces machined by the TTs and CTs increased.

4. Discussion

In this study, derivative cutting of TTs was investigated. Results showed that the workpiece machined by the derivative cutting showed smaller surface roughness and smoother surface

topography than the conventionally processed workpiece. Derivative cutting can remove part of the fine grain zone of the machined surface, leading to a thinner depth of the fine grain zone and smaller work-hardening values than the surface machined by CTs.

Derivative cutting is a phenomenon of microcutting because the dimensions of the microscale texture and the surface defects produced during machining are comparable in size (Ref 16). A schematic of the derivative cutting is shown in Fig. 24. As depicted in Fig. 24(b), when the height of the protuberances (h)

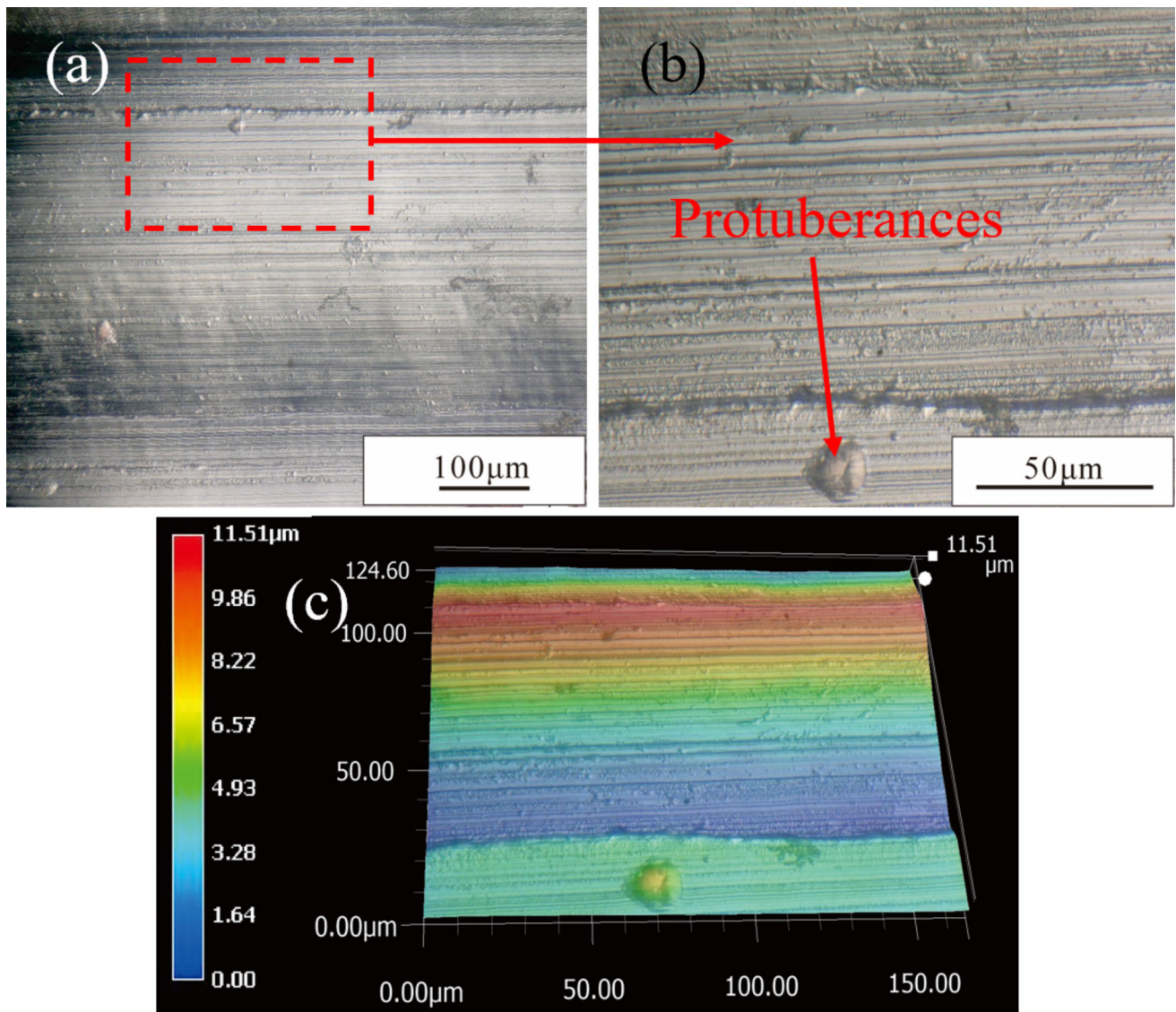


Fig. 15 Surface topography with CT at 270 m/min. (a) Surface topography, (b) magnified view of (a), and (c) 3D profile of (b)

on the machined surface was less than the minimum chip thickness (h_{\min}), elastic deformation occurred on the machined surface without the formation of derivative chips. Derivative cutting plays a role in the ironing of machined surfaces. When the height of the protuberances was greater than the minimum chip thickness, plastic deformation took place on the machined surface. This resulted in the formation of derivative chips, as shown in Fig. 24(c). Derivative cutting can remove part of the surface materials from the workpiece. The surface materials

contained microscopic defects and fine grain zone with a strong strain-hardening layer (Ref 28), leading to a decrease in surface roughness, a reduction in the depth of the fine grain zone, and a weakening of the work-hardening values of the machined surface. Additionally, the derivative cutting reduces the negative influence of machining defects on the unworn tool face and enhances the wear resistance of tools with textured flank face.

According to the analysis of all the samples, the effect of derivative cutting on the hardness values of the surface and the

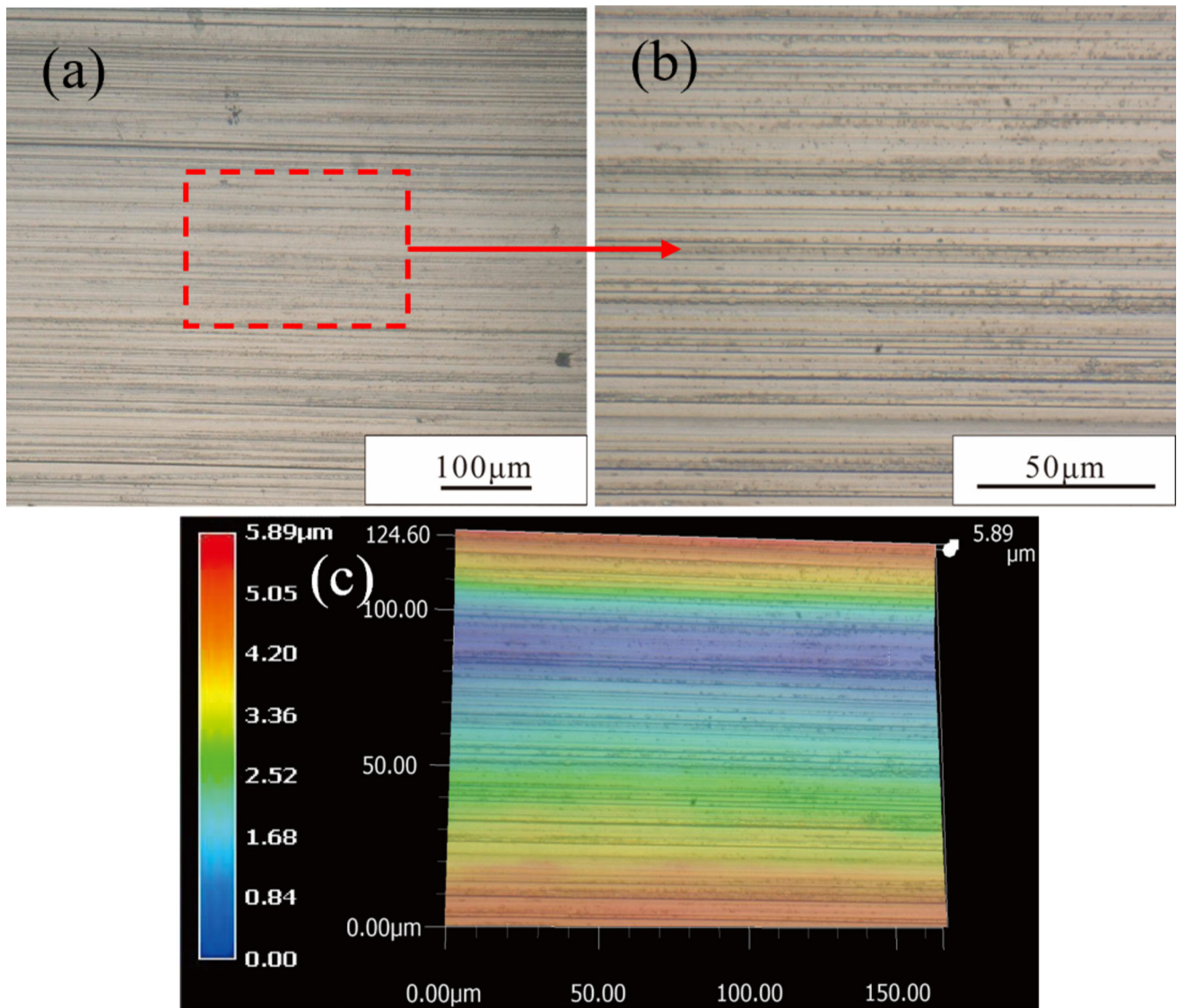


Fig. 16 Surface topography with TT at 90 m/min. (a) Surface topography, (b) magnified view of (a), and (c) 3D profile of (b)

roughness of the surface was evident with increasing cutting velocity. For the surface machined by the CTs, the thermo-mechanical loads at the contact interface increased in the cutting velocity range of 90 to 270 m/min, which led to the enhancement of plastic flow on the machined surface. The plastic flow of the workpiece materials causes them to build up

on the machined surface (Ref 29), which increases the surface roughness, as illustrated in Fig. 20. However, derivative cutting removes the materials build-up on the machined surface and iron it, as for the surface machined by TTs. Derivative cutting occurred intensively, causing the microtexture to be buried with derivative chips (Fig. 10) at a high cutting velocity. This results

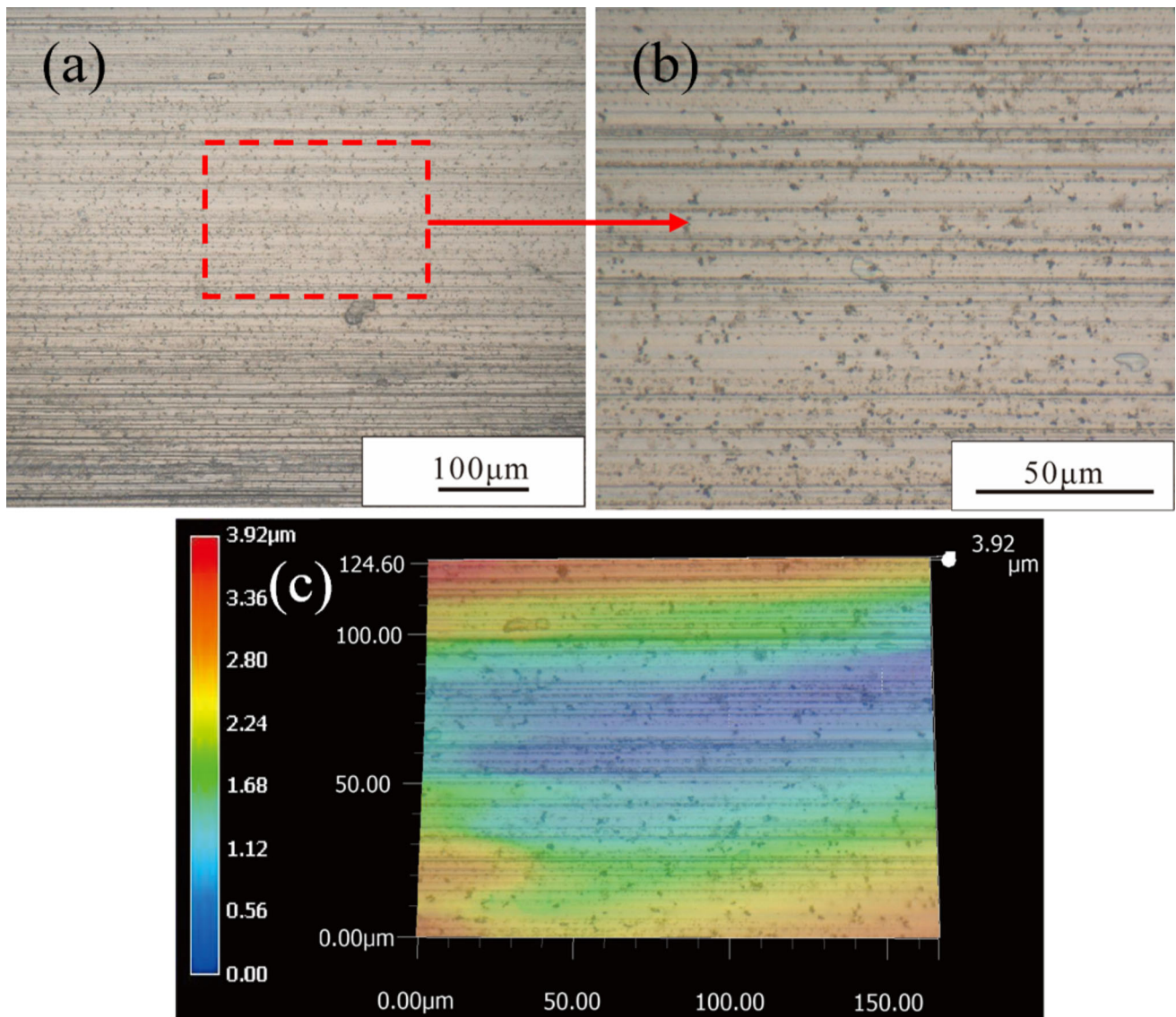


Fig. 17 Surface topography with TT at 133 m/min. (a) Surface topography, (b) magnified view of (a), and (c) 3D profile of (b)

in a significant reduction in the surface roughness. In addition, for the work hardening of workpieces machined by TTs, intensive derivative cutting removes a part of the fine grain zone containing a strong strain-hardening layer. Therefore, there are evident differences between the surfaces machined by

the TTs and those machined by the CTs within the span of cutting velocity, from 133 to 270 m/min.

The machined surface is significantly influenced by the bottom edge of texture acting as a “cutting edge.” Figure 3 clearly demonstrates noticeable chipping occurring at cutting

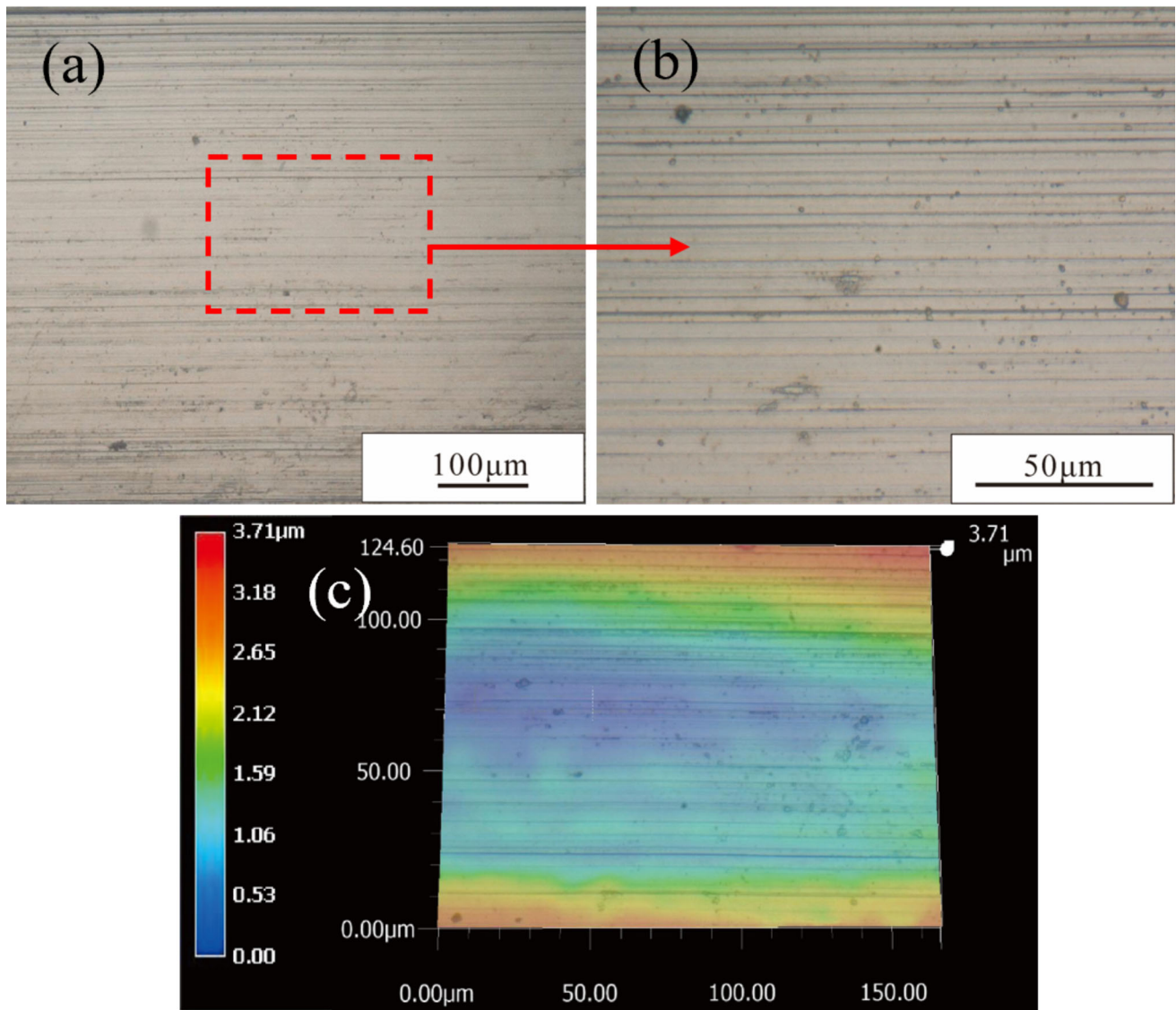


Fig. 18 Surface topography with TT at 211 m/min. (a) Surface topography, (b) magnified view of (a), and (c) 3D profile of (b)

velocity of 90 m/min, owing to intensive vibrations and shocks during the cutting process. The wear zone on the flank face, when in contact with the workpiece surface, rubbed against the machined surface. This caused the defects of the plowing grooves on the machined surface (Fig. 12). However, there were no clear defects on the surface machined using the

chipped TTs. Therefore, for TTs, the main cutting edge of sudden failure will be timely replaced by the bottom edge of texture. Additionally, the formation of a temporary “cutting edge” can prolong the lifespan of ceramic tools, which is advantageous for enhancing the surface quality of the workpiece.

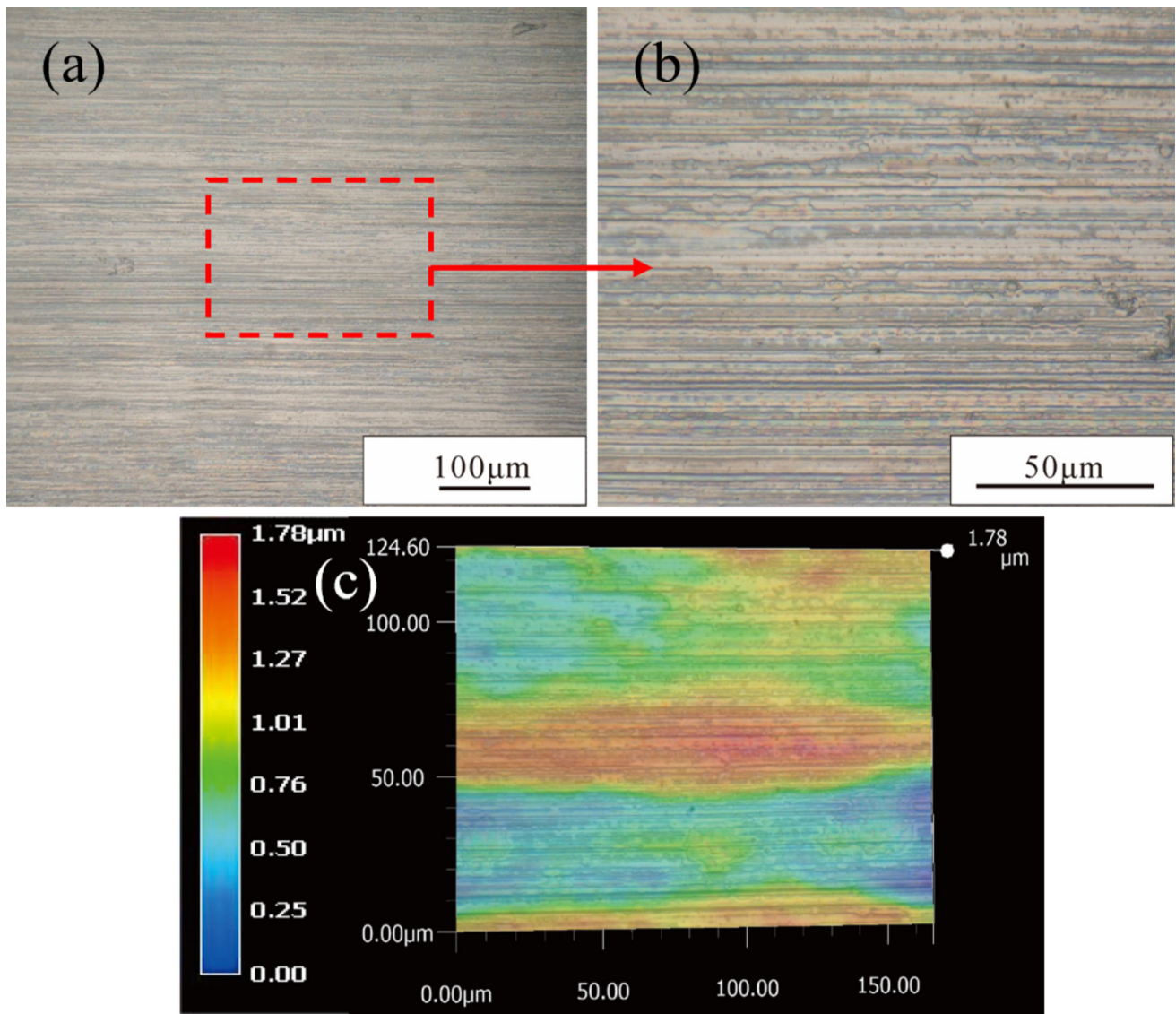


Fig. 19 Surface topography with TT at 270 m/min. (a) Surface topography, (b) magnified view of (a), and (c) 3D profile of (b)

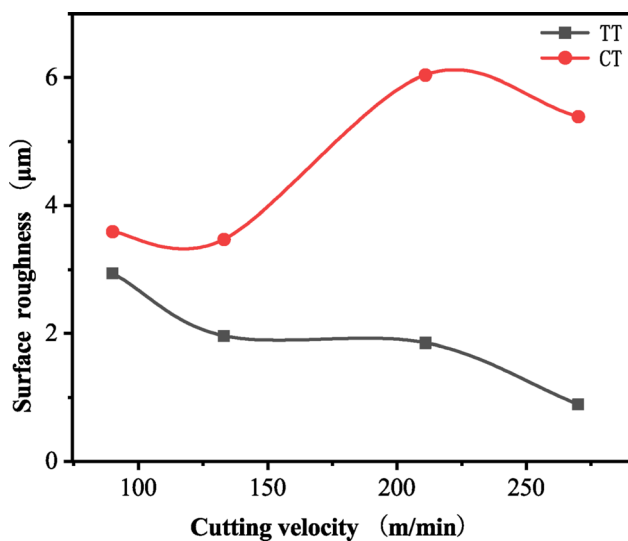


Fig. 20 Variations in surface roughness with the cutting velocity obtained with CTs and TTs

Based on the analysis presented, the TTs affect the surface quality of the workpiece by derivative cutting and friction reduction of the flank-faced texture (Ref 30-32) over the cutting velocity interval from 90 to 211 m/min. The machined surface of the workpiece was primarily affected by derivative cutting, owing to the plugged microtexture at 270 m/min. With an increase in cutting velocity, the derivative cutting has a significant effect on reducing the surface roughness and work-hardening values.

5. Conclusion

In this research, an Al_2O_3 ceramic tool with a microgroove on the flank face was created. The microgroove was paralleled to the main cutting edge. Dry-cutting experiments were

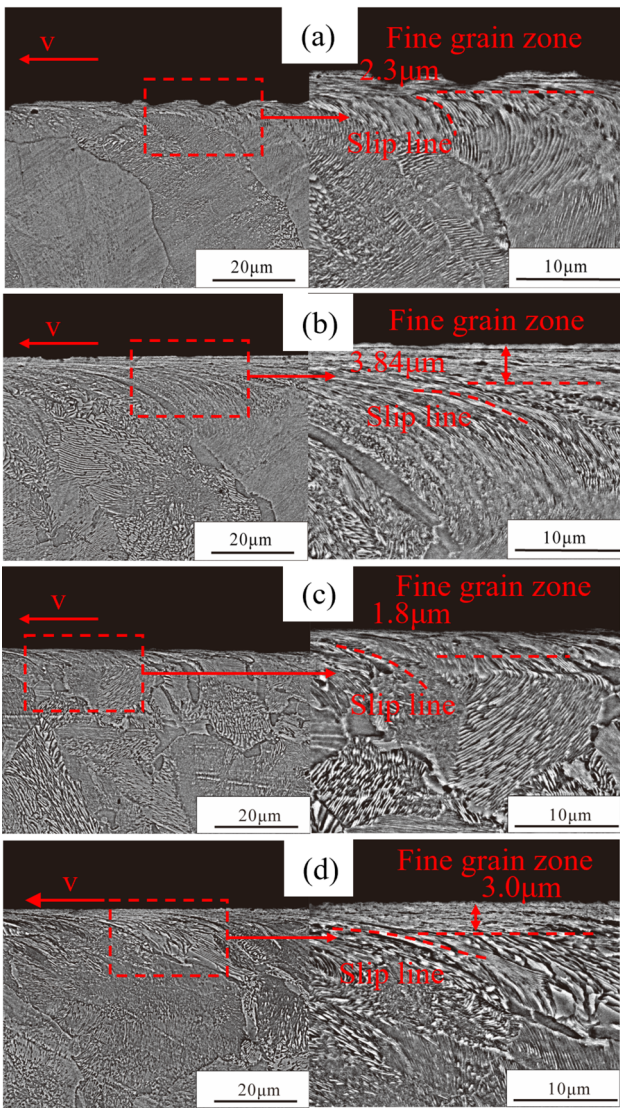


Fig. 21 Microstructure of the AISI 1045 obtained with CTs at various cutting velocity. (a) 90 m/min, (b) 133 m/min, (c) 211 m/min, and (d) 270 m/min

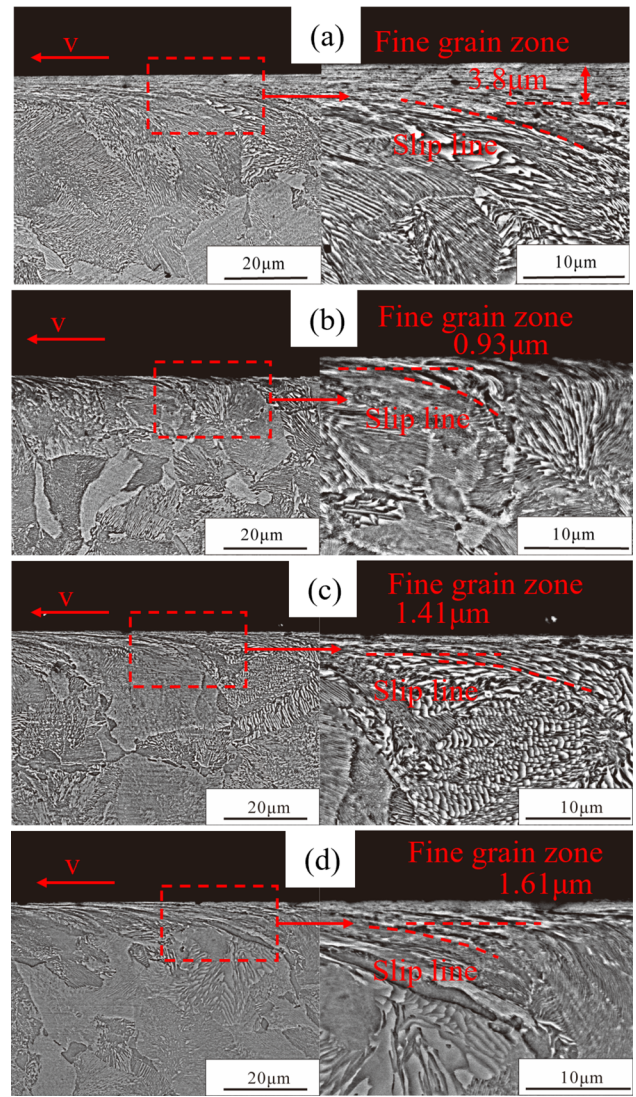


Fig. 22 Microstructure of the AISI 1045 obtained with TTs at various cutting velocity. (a) 90 m/min, (b) 133 m/min, (c) 211 m/min, and (d) 270 m/min

performed using TTs and CTs. The following conclusions were drawn:

- (1) Derivative cutting of the flank-faced textured ceramic tools occurs at cutting velocities ranging from 90 to 270 m/min, leading to a decrease in surface roughness, a reduction in the depth of the fine grain zone, and a weakening of the work hardening of the surface compared with those of the surface machined by CTs.
- (2) Derivative cutting has a pronounced impact on the surface roughness with increased cutting velocity, owing to the fact that most of the materials build-up on the machined surface caused by the plastic flow at a high cutting velocity is removed by derivative cutting.
- (3) The bottom edge of the texture as a “cutting edge” can timely substitute for the main cutting edge of sudden failure, extending the tools lives and improving the surface quality.

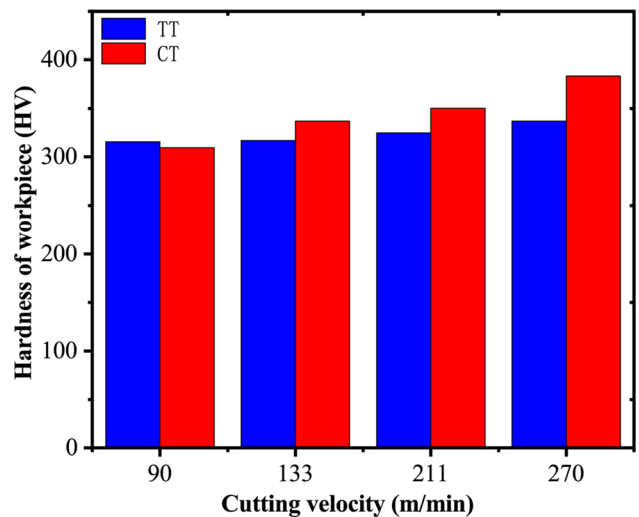


Fig. 23 Hardness of workpiece machined with CTs and TTs

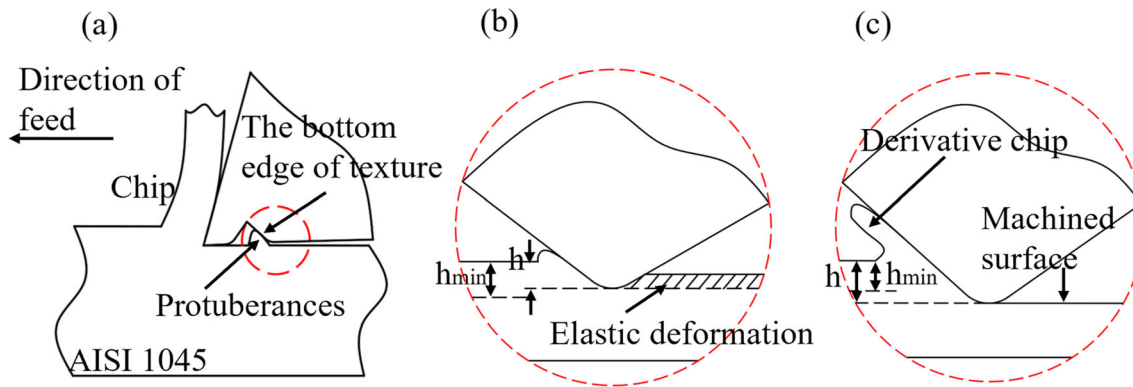


Fig. 24 Schematic diagram of derivative cutting

Acknowledgments

Special thanks to the Doctoral Foundation of Shandong Jianzhu University (X20058Z0101).

References

- P. Ranjan and S.S. Hiremath, Role of Textured Tool in Improving Machining Performance: A Review, *J. Manuf. Process.*, 2019, **43**, p 47–73
- C.H. Kumar and S.K. Patel, Application of Surface Modification Techniques during Hard Turning: Present Work and Future Prospects, *Int. J. Refract. Met. Hard Mater.*, 2018, **76**, p 112–127
- A.R. Machado, L.R.R. Silva, F.C.R. Souza, R.D.L.C. Pereira, W.F. Sales, W. Rossi, and E.O. Ezugwu, State of the Art of Tool Texturing in Machining, *J. Mater. Process. Technol.*, 2021, **293**, p 117076
- J. Xie, M.J. Luo, J.L. He, X.R. Liu, and T.W. Tan, Micro-grinding of Micro-groove Array on Tool Rake Surface for Dry Cutting of Titanium Alloy, *Int. J. Precis. Eng. Manuf.*, 2012, **13**(10), p 18452–21852
- J. Ma, N.H. Duong, S. Chang, Y. Lian, J. Deng, and S. Lei, Assessment of Microgrooved Cutting Tool in Dry Machining of AISI 1045 Steel, *J. Manuf. Sci. Eng.*, 2015, **137**, p 03100–03101
- D. Jianxin, L. Yunsong, W. Ze, and X. Youqiang, Performance of Femtosecond Laser-Textured Cutting Tools Deposited with WS₂ Solid Lubricant Coatings, *Surf. Coat. Technol.*, 2013, **222**, p 135–143
- B. Qi and L. Li, Experimental Study on Orthogonal Cutting of Ti6Al4V with Surface Micro-groove Textured Cutting Tool, *Mater. Sci. Forum*, 2012, **723**, p 243–246
- J. Xie, M.J. Luo, K.K. Wu, L.F. Yang, and D.H. Li, Experimental Study on Cutting Temperature and Cutting Force in Dry Turning of Titanium Alloy Using a Non-coated Micro-grooved Tool, *Int. J. Mach. Tools Manuf.*, 2013, **73**, p 25–36
- S. Lei, S. Devarajan, and Z. Chang, A comparative Study on the Machining Performance of Textured Cutting Tools with Lubrication, *Int. J. Mech. Manuf. Syst.*, 2009, **2**(4), p 401–413
- A. Fatima and P.T. Mativenga, A Comparative Study on Cutting Performance of Rake-Flank Face Structured Cutting Tool in Orthogonal Cutting of AISI/SAE 4140, *Int. J. Adv. Manuf. Technol.*, 2015, **78**(9–12), p 2097–2106
- S.K. Rajbongshi, M.A. Singh, and D.K. Sarma, A Comparative Study in Machining of AISI D2 Steel Using Textured and Non-textured Coated Carbide Tool at the Flank Face, *J. Manuf. Process.*, 2018, **36**, p 360–372
- W. Ze, D. Jianxin, C. Yang, X. Youqiang, and Z. Jun, Performance of the Self-Lubricating Textured Tools in Dry Cutting of Ti-6Al-4V, *Int. J. Adv. Manuf. Technol.*, 2012, **62**, p 943–951
- S.K. Rajbongshi and D.K. Sarma, Performance Parameters Studies in Machining of AISI D2 Steel with Dot-Textured, Groove-Textured & Non-textured Cutting Tool at the Flank Face, *Int. J. Refract. Met. H.*, 2019, **83**, p 104970
- M. Muaz and S.K. Choudhury, Enhancing the Tribological Aspects of Machining Operation by Hybrid Lubrication-Assisted Side-Flank-Face Laser-Textured Milling Insert, *J. Braz. Soc. Mech. Sci. Eng.*, 2019, **41**, p 527
- T. Sugihara, Y. Nishimoto, and T. Enomoto, Development of a Novel Cubic Boron Nitride Cutting Tool with a Textured Flank Face for High-Speed Machining of Inconel 718, *Precis. Eng.*, 2017, **48**, p 75–82
- P. Ranjan and S. Hiremath, Influence of Texture Parameters of the Bio-inspired Crescent Textured Tool on Machining Performance of Martensitic Stainless Steel, *CIRP J. Manuf. Sci. Technol.*, 2022, **39**, p 70–90
- R. Duan, J. Deng, S. Lei, D. Ge, Y. Liu, and X. Li, Effect of Derivative Cutting on Machining Performance of Micro Textured Tools, *J. Manuf. Process.*, 2019, **45**, p 544–556
- Y. Liu, J. Deng, W. Wang, R. Duan, R. Meng, D. Ge, and X. Li, Effect of Texture Parameters on Cutting Performance of Flank-Faced Textured Carbide Tools in Dry Cutting of Green Al₂O₃ Ceramics, *Ceram. Int.*, 2018, **44**(11), p 13205–13217
- R. Xu and Y. Yongfeng, Effect of Micro-texture of Flank Surface on Broaching Force and Surface Quality of Workpiece, *Appl. Surf. Sci.*, 2020 <https://doi.org/10.1016/j.apsusc.2020.146558>
- Y. Liu, J. Deng, F. Wu, R. Duan, X. Zhang, and Y. Hou, Wear Resistance of Carbide Tools with Textured Flank-Face in Dry Cutting of Green Alumina Ceramics, *Wear*, 2017, **372–373**, p 91–103
- R. Duan, J. Deng, S. Lei, D. Ge, Y. Liu, and X. Li, A Study on New Surface Textured Tools for Inhibition of Derivative Cutting, *J. Manuf. Sci. Eng.*, 2019, **141**(12), p 124501
- X. Wang, V.L. Popov, Z. Yu, Y. Li, J. Xu, Q. Li, and H. Yu, Evaluation of the Cutting Performance of Micro-groove-textured PCD Tool on SiCp/Al Composites, *Ceram. Int.*, 2022, **48**(21), p 32389–32398
- Y. Xing, J. Deng, J. Zhao, G. Zhang, and K. Zhang, Cutting Performance and Wear Mechanism of Nanoscale and Microscale Textured Al₂O₃/TiC Ceramic Tools in Dry Cutting of Hardened Steel, *Int. J. Refract. Met. Hard Mater.*, 2014, **43**, p 46–58
- Y. Liu, J. Deng, W. Wang, R. Duan, and Y. Xing, Characterization of Green Al₂O₃ Ceramics Surface Machined by Tools with Textures on Flank-Face in Dry Turning, *Int. J. Appl. Ceram. Technol.*, 2019, **16**, p 1159–1172
- R. Duan, G. Wang, and Y. Xing, Investigation of Novel Multiscale Textures for the Enhancement of the Cutting Performance of Al₂O₃/TiC Ceramic Cutting Tools, *Ceram. Int.*, 2022, **48**(3), p 3554–3563
- G. Zhang, S. To, and S. Zhang, Relationships of Tool Wear Characteristics to Cutting Mechanics, Chip Formation, and Surface Quality in Ultra-Precision Fly Cutting, *Int. J. Adv. Manuf. Technol.*, 2016, **83**(1–4), p 133–144
- D. Jianxin, W. Ze, L. Yunsong, Q. Ting, and C. Jie, Performance of Carbide Tools with Textured Rake-Face Filled with Solid Lubricants in Dry Cutting Processes, *Int. J. Refract. Met. Hard Mater.*, 2012, **30**(1), p 164–172
- K. Gao, X. Qin, Z. Wang, and S. Zhu, Effect of Spot Continual Induction Hardening on the Microstructure of Steels: Comparison Between AISI 1045 and 5140 Steels, *Mat. Sci. Eng. A*, 2016, **651**, p 535–547
- J. Yu, G. Wang, and Y. Rong, Experimental Study on the Surface Integrity and Chip Formation in the Micro Cutting Process, *Proc. Manuf.*, 2015, **1**, p 655–662

30. V. Sharma and P.M. Pandey, Recent Advances in Turning with Textured Cutting Tools: A Review, *J. Clean. Prod.*, 2016, **137**, p 701–715
31. K. Zhang, J. Deng, Y. Xing, S. Li, and H. Gao, Effect of Microscale Texture on Cutting Performance of WC/Co-Based TiAlN Coated Tools Under Different Lubrication Conditions, *Appl. Surf. Sci.*, 2015, **326**, p 107–118
32. D.M. Kim, I. Lee, S.K. Kim, B.H. Kim, and H.W. Park, Influence of a Micropatterned Insert on Characteristics of the Tool-Workpiece Interface in a Hard Turning Process, *J. Mater. Process. Technol.*, 2016, **229**, p 160–171

Publisher's Note Springer Nature remains neutral with regard to jurisdictional claims in published maps and institutional affiliations.

Springer Nature or its licensor (e.g. a society or other partner) holds exclusive rights to this article under a publishing agreement with the author(s) or other rightsholder(s); author self-archiving of the accepted manuscript version of this article is solely governed by the terms of such publishing agreement and applicable law.